

# Fast detection of single-charge tunneling to a graphene quantum dot in a multi-level regime

T. Müller<sup>\*†</sup>, J. Güttinger<sup>‡</sup>, D. Bischoff, S. Hellmüller, K. Ensslin, and T. Ihn  
*Solid State Physics Laboratory, ETH Zürich, 8093 Zürich, Switzerland*  
 (Dated: June 7, 2018)

*In situ*-tunable radio-frequency charge detection is used for the determination of the tunneling rates into and out of a graphene single quantum dot connected to only one lead. An analytical model for calculating these rates in the multi-level tunneling regime is presented and found to correspond very well to our experimental observations.

PACS numbers: 73.23.Hk, 72.80.Vp, 85.35.Be

Keywords: Charge detection, radio frequency, graphene, quantum dot, single-charge tunneling, multi-level tunneling

Time-resolved charge detection on quantum dots is a powerful technique to straightforwardly extract single-particle transport properties such as the occupation probability of quantum dots determined by the Fermi distribution function in the leads and the dot-lead tunneling rates [1, 2]. Recording the charge-detector signal through radio-frequency (rf) reflection measurements [3] can enhance the time resolution drastically, enabling studies of systems with larger tunneling rates.

To date, these types of experiments mainly study quantum dots in the single-level regime, and investigations involving transport through more than one level have focused on the phenomenon of super-Poissonian noise [4–6]. Here, we present measurements and an analytical calculation of multi-level tunneling rates using a graphene single quantum dot connected to one lead.

Our charge-detection experiments were performed by incorporating a graphene nanoconstriction charge detector, capacitively coupled to a graphene single quantum dot, into an *in situ*-tunable resonant circuit [7]. A schematic view of the latter and an atomic force microscopy image of the former are presented in Figs. 1(a) and (b), respectively. The structure was fabricated through reactive ion etching on a mechanically exfoliated graphene flake [8]. The parts of the graphene flake etched away are emphasized by dashed black lines in Fig. 1(b) to enhance visibility. The roughly 100 nm sized quantum dot (marked by the dashed red ellipse) and the nanoconstriction (designated by the single-sided arrow) can be tuned by in-plane gates and a global backgate. In spite of the symmetric design of the barriers forming the quantum dot, only the upper lead (source; represented by the double-sided arrow) was tunnel-coupled to the dot. Therefore, we were not able to measure direct transport through the graphene quantum dot. A more detailed

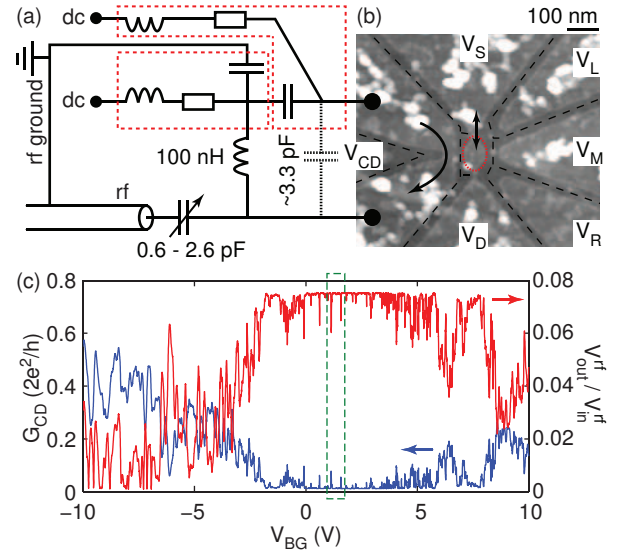


FIG. 1: (Color online) (a) Schematic representation of the circuitry used for rf and dc measurements. The dotted black capacitor is the total stray capacitance, and the dashed red boxes enclose on-chip bias tees allowing for separation of low- and high-frequency signals. (b) Atomic force microscopy image of the graphene device studied in our experiments. Dashed black lines mark regions of graphene etched away to form a nanoconstriction at the location of the single-sided arrow and a quantum dot encircled in dashed red. The nanoconstriction charge detector is attached to the resonant circuit as a resistive element  $R$ . (c) Conductance of the nanoconstriction measured via dc current (blue trace, left axis) and rf reflectometry (red trace, right axis).

description of the fabrication procedure for this kind of devices can be found in Ref. [9].

Due to the large stray capacitance formed between the metallic bond pads and the highly doped silicon backgate, high-quality rf matching of graphene samples using the standard circuit design forming a resonance between a series inductor and the total stray capacitance is difficult. One way to avoid this challenge is to remove the backgate underneath the bond pads, which

<sup>\*</sup>Electronic address: thommuel@phys.ethz.ch

<sup>†</sup>Present address: Department of Chemistry, University of Cambridge, Cambridge CB2 1EW, UK

<sup>‡</sup>Present address: CIN2 (ICN-CSIC), Catalan Institute of Nanotechnology, Campus de la UAB, 08193 Bellaterra (Barcelona), Spain

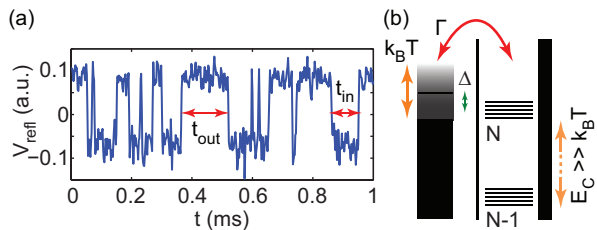


FIG. 2: (Color online) (a) Time-dependent rf signal, 8-th order Bessel low-pass filtered at 200 kHz and sampled at 500 kHz, revealing the times  $t_{\text{in}}$  and  $t_{\text{out}}$  the quantum dot is occupied or unoccupied by a single negative excess charge. (b) Sketched energy diagram corresponding to the multi-level regime studied here. A quantum dot with a closely-spaced energy spectrum is connected to a lead with a tunnel rate  $\Gamma$ . The Fermi function of the lead is softened by a temperature  $T$  which is much larger than the level spacing  $\Delta E$  but much smaller than the charging energy  $E_C$ . The difference between the Fermi level in the lead and the chemical potential of the quantum dot is denoted by  $\Delta$ .

however complicates the already involved fabrication of graphene nanostructures. We chose an alternative circuit design consisting of a tunable capacitance in series to a parallel  $LCR$  circuit [7]. Doing so and harnessing the large change in conductance of the nanoconstriction upon addition of a single charge to the quantum dot due to the proximity of the structures ( $\Delta G \approx 0.08 \times 2e^2/h$  at  $G \sim 0.1 \times 2e^2/h$ ) yields a very good charge sensitivity of  $\delta q \approx 3 \times 10^{-4} e/\sqrt{\text{Hz}}$  [7, 10–13].

All our measurements were performed in a variable-temperature insert at a temperature of roughly 2 K.

The blue curve in Fig. 1(c) shows the dc conductance (left axis) through the nanoconstriction charge sensor as a function of backgate voltage, while the red curve is the simultaneously acquired rf reflection coefficient. Both measurements reveal a transport gap in the backgate range between around  $-1$  and  $4$  V. Subsequent measurements are performed in the regime of the dashed green box, in proximity of the charge-neutrality point of the graphene charge sensor [14].

Tuning all gate voltages such that the quantum dot is at a charge-degeneracy point between  $N - 1$  and  $N$  negative charges on the dot [15] and recording the charge-detector conductance via rf reflectometry allows for studying tunneling of single charge carriers in real-time, as shown in Fig. 2(a). This trace has been 8-th order Bessel low-pass filtered at 200 kHz - roughly two orders of magnitude faster than with previous time-resolved experiments on graphene quantum dots [16] - and sampled at 500 kHz to ensure large enough signal-to-noise ratio for reliable electron counting [17]. From the average time a negative charge spends inside (out of) the dot we can compute the dot occupation probability and the rate for tunneling out of (into) the quantum dot.

At our elevated temperatures we have good reason [18] to assume that we are in a multi-level tunneling regime - an assumption that we will show to be correct in our dis-

cussion of the experimental data. Thus we now calculate the tunneling rates of a quantum dot connected to one lead in the multi-level regime schematized in Fig. 2(b). Our analysis closely follows the work of Beenakker [19] in which all the ingredients for the subsequent analysis are provided, and we also adopt the notation thereof.

The multi-level regime of Coulomb blockade is characterized by a temperature  $k_B T$  much larger than the single-level spacing  $\Delta E$  but much smaller than the charging energy  $E_C$

$$\Delta E \ll k_B T \ll E_C. \quad (1)$$

The latter inequality is validated by the fact that we extracted an approximate charging energy of  $10 - 20$  meV typical for graphene quantum dots of this size (see for instance Ref. [16]), whereas we assume the former to be true since we have not observed any sign of excited states in either the similarly sized charge detector or the dot itself. Nevertheless, we shall assert the inequality's validity later-on.

It has been shown in Ref. [19] that the rate for tunneling into a quantum dot occupied by  $N - 1$  charges is given by the sum over all quantum dot states  $p$  of their respective couplings  $\Gamma_p$  multiplied by the probability to have a state at energy  $E_p$  available in the lead (given by the Fermi distribution function  $f$ ) and the conditional probability  $1 - F_{\text{eq}}(E_p|N - 1)$  of having state  $p$  empty in an  $N - 1$ -fold occupied dot in equilibrium

$$\Gamma_{\text{in}} = \sum_p \Gamma_p [1 - F_{\text{eq}}(E_p|N - 1)] \times f(E_p + U_N - U_{N-1} - E_F), \quad (2)$$

where  $U_N$  is the electrostatic energy of a dot containing  $N$  negative charge carriers, and  $E_F$  is the chemical potential in the lead(s). Beenakker has also elucidated that  $F_{\text{eq}}(E_p|N)$  can be expressed as a Fermi function  $f(E_p - \mu_N)$  in the high-temperature limit, where the chemical potential  $\mu_N$  of the dot is determined by

$$\sum_{p=0}^{\infty} f(E_p - \mu_N) = N. \quad (3)$$

By assuming the couplings  $\Gamma_p$  to be equal and independent of energy, we can replace the sum by an integral over energy times density of states  $\rho$  which we will also assume to be energy-independent. Thus we can perform the integration which yields

$$\begin{aligned} \Gamma_{\text{in}} &= \frac{\rho \Gamma [-U_N + U_{N-1} + E_F - \mu_{N-1}]}{1 - \exp[(U_N - U_{N-1} - E_F + \mu_{N-1})/k_B T]} \\ &\equiv \rho \Gamma \frac{\Delta}{1 - \exp(-\Delta/k_B T)}, \end{aligned} \quad (4)$$

where  $\Delta$  is the energy detuning between the chemical potentials in the lead and the dot (note that our definition of  $\Delta$  has an additional minus sign compared to the one

of Ref. [19]). Analogously, we can compute

$$\begin{aligned}\Gamma_{\text{out}} &= \sum_p \Gamma_p F_{\text{eq}}(E_p|N) \\ &\quad \times [1 - f(E_p + U_N - U_{N-1} - E_F)] \\ &= \rho\Gamma \frac{-\Delta}{1 - \exp(\Delta/k_B T)}.\end{aligned}\quad (5)$$

In this last equality we have made use of the fact that at our relevant energies  $\mu_{N-1} \approx \mu_N$ .

Adding these two expressions leads to the inverse of the correlation time of the random telegraph signal [20] given by

$$\gamma = \Gamma_{\text{in}} + \Gamma_{\text{out}} = \Gamma\rho\Delta \frac{\sinh(\Delta/k_B T)}{\cosh(\Delta/k_B T) - 1}.\quad (6)$$

We want to emphasize that in contrast to the above expression, the sum of tunnel rates is constant with respect to detuning in the single-level regime if the couplings for tunneling-in and -out are equal (and are only varying over a range of the order of  $k_B T$  otherwise). Therefore, a strongly varying sum of tunneling rates excludes a single-level regime.

The expected rate of events  $r_E$  (the number of times per second an electron tunnels in and out of the quantum dot) can now be calculated to be

$$\begin{aligned}r_E &= \frac{\Gamma_{\text{in}}\Gamma_{\text{out}}}{\Gamma_{\text{in}} + \Gamma_{\text{out}}} = \frac{\Gamma\rho\Delta}{2 \sinh(\Delta/k_B T)} \\ &\approx \frac{\Gamma\rho}{2} \frac{\Delta}{k_B T} \cosh^{-2}\left(\frac{\Delta}{2.5k_B T}\right),\end{aligned}\quad (7)$$

equivalent to what Beenakker found for the conductance through a dot in the multi-level regime (and what Kulik and Shekhter found for transport through granular metals [21]) since in all instances, tunneling-in and -out are treated on an equal footing.

Equipped with these analytical expressions for the tunneling rates, we turn to our experimental results. Figure 3(a) shows the fraction of time the quantum dot is devoid of the  $N$ -th excess charge when sweeping over the  $\{N-1, N\}$  charge-degeneracy point, reflecting the Fermi distribution function of the lead. Fitting the measured data (blue dots) with a Fermi function (solid black curve) results in a temperature of  $T = 1.97 \pm 0.03$  K. Using this temperature, we can compare the number of tunneling events extracted from the same time traces with the expected number in a single- (dashed green line; see Ref. [19]) and multi-level (solid red line; Eq. 7) regime in Fig. 3(b). We find that the solid red line corresponding to multi-level tunneling matches the measurements better [22].

In Fig. 3(c) we show the experimentally extracted rates for tunneling-in (blue circles) and tunneling-out (red crosses). Additionally, we plot the analytical functions for the rates given by Eqs. 4 and 5 as solid lines. The only fit parameter for these curves is the product  $\Gamma\rho$  of tunnel coupling and density of states which was

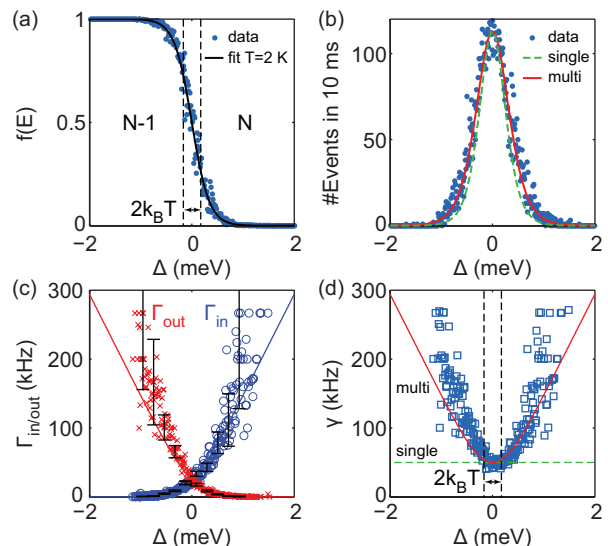


FIG. 3: (Color online) (a) Electronic occupancy of the lead as a function of dot-lead energy detuning  $\Delta$ . Every blue data point is the fraction of time the dot is occupied by  $N-1$  (instead of  $N$ ) negative charges as extracted from traces as shown in Fig. 2(a). The solid black line is a fit to a Fermi distribution function in the lead, yielding a temperature of  $T = 1.97 \pm 0.03$  K. The dashed black lines indicate the magnitude of temperature. (b) Number of tunneling events in a 10 ms long trace. The dashed green and solid red lines are calculated rates for a single and multi-level regime, respectively, using the temperature extracted in (a) and the height of the data points. (c) Tunneling rates determined through the average dwell times in (red crosses) and out (blue circles) of the quantum dot. The solid lines are calculations using Eqs. 4 and 5 in the main text. For sake of clarity, the statistical error bars are only shown for one in 20 traces. (d) Measured (blue squares) and analytically determined (Eq. 6; solid red line) sum of the multi-level tunnel rates shown in (c). The dotted green line indicates the behavior in the single-level regime.

chosen such that the experimental results coincide with the calculations at zero detuning. The error bars indicating the uncertainty of the determination of the tunneling rates from the dwell times [5] are only shown for one in 20 data points to enhance visibility. Finally, the sum of these tunneling rates is presented in Fig. 3(d) for both, experiment (blue squares) and single- (dotted green line) as well as multi-level (solid red line; Eq. 6) models. As we observe a linear increase in the sum of the rates for detunings above  $k_B T$ , we can be certain to be in a multi-level regime.

In all plots of Fig. 3, the horizontal axis has been converted to energy using a lever arm set via the relative influence of the swept backgate and the dot source lead [23].

The qualitative and quantitative agreement between our experiments and theoretical calculations is striking, especially considering that only one free parameter  $\Gamma\rho$  is available, since temperature has been fixed by the Fermi fit in (a). Nevertheless, we observe a deviation from the model for large detuning, where the experimentally ob-

tained values lie distinctly above our expectations. This may originate from the fact that, in contrast to our assumptions, either the density of states  $\rho$  or the tunnel couplings  $\Gamma_p$  in the dot are not entirely independent of energy. Furthermore, the couplings may be different for each state  $p$ . Also, it is conceivable that only a finite number of states contribute to tunneling. From the energy-dependence of the sum of tunneling rates in Fig. 3(d), though, we can definitely exclude single-level tunneling. Missed events due to our large yet finite bandwidth lead to a further enhancement of the numeric value of the measured tunnel rates for large  $\Delta$  and can therefore not explain the deviations.

In conclusion we have performed time-resolved charge detection measurements on a graphene quantum dot us-

ing rf reflectometry with large bandwidth. From these experiments we have extracted the rates for tunneling-in and tunneling-out of the dot, which are in good agreement with our analytical model for multi-level tunneling to a single lead. This type of fast charge detection on graphene quantum dots opens possibilities for studying interactions of Dirac Fermions in the framework of full counting statistics and is a great instrument for determining spin relaxation times in graphene quantum dot circuits.

We thank C. Barengo for invaluable technical assistance and B. Küng and Y. Komijani for fruitful discussions. Funding by the Swiss National Science Foundation (SNF) via National Center of Competence in Research (NCCR) Nanoscale Science is gratefully acknowledged.

- 
- [1] R. Schleser, E. Ruh, T. Ihn, K. Ensslin, D. C. Driscoll, and A. C. Gossard, *Appl. Phys. Lett.* **85**, 2005 (2004)
  - [2] L. M. K. Vandersypen, J. M. Elzermann, R. N. Schouten, L. H. Willems van Beveren, R. Hanson, and L. P. Kouwenhoven, L. P., *Appl. Phys. Lett.* **85**, 4394 (2004)
  - [3] R. J. Schoelkopf, P. Wahlgren, A. A. Kozhenikov, P. Delsing, and D. E. Prober, *Science* **280**, 1238 (1998)
  - [4] W. Belzig, *Phys. Rev. B* **71**, 161301(R) (2005)
  - [5] S. Gustavsson, R. Leturcq, B. Simović, R. Schleser, P. Studerus, T. Ihn, K. Ensslin, D. C. Driscoll, and A. C. Gossard, *Phys. Rev. B* **74**, 195305 (2006)
  - [6] C. Fricke, F. Hohls, W. Wegscheider, and R. J. Haug, *Phys. Rev. B* **76**, 155307 (2007)
  - [7] T. Müller, B. Küng, S. Hellmüller, P. Studerus, K. Ensslin, T. Ihn, M. Reinwald, and W. Wegscheider, *Appl. Phys. Lett.* **97**, 202104 (2010)
  - [8] K. Novoselov, A. K. Geim, S. V. Morozov, D. Jiang, Y. Zhanh, S. V. Dubonos, I. V. Grigorieva, A. A. Firsov, *Science* **306** 666 (2004)
  - [9] J. Güttinger, C. Stampfer, T. Frey, T. Ihn, and K. Ensslin, *Phys. Status Solidi* **246**, 2553 (2009)
  - [10] I. T. Vink, T. Nooitgedagt, R. N. Schouten, L. M. K. Vandersypen, and W. Wegscheider, *Appl. Phys. Lett.* **91** 123512 (2007)
  - [11] D. J. Reilly, C. M. Marcus, M. P. Hanson, and A. C. Gossard, *Appl. Phys. Lett.* **91**, 162101 (2007)
  - [12] M. C. Cassidy, A. S. Dzurak, R. G. Clark, K. D. Petersson, I. Farrer, D. A. Ritchie, and C. G. Smith, *Appl. Phys. Lett.* **91**, 222104 (2007)
  - [13] C. Barthel, M. Kjærgaard, J. Medford, M. Stopa, C. M. Marcus, M. P. Hanson and A. C. Gossard, *Phys. Rev. B* **87**, 161308(R) (2010)
  - [14] Since the charge sensor and the quantum dot were fabricated from the same flake it seems fair to assume the Dirac points of both devices to be rather close. Thus, we have chosen settings close to the detector's charge-neutrality point, where the low density of states should result in small enough tunneling rates.
  - [15] From Fig. 1(c) we may expect to be in the hole regime. Nevertheless, we are always referring to single negative charges being added to the dot (removal of a hole) in order to avoid confusion.
  - [16] J. Güttinger, J. Seif, C. Stampfer, A. Capelli, K. Ensslin, and T. Ihn, *Phys. Rev. B* **83**, 165445 (2011)
  - [17] S. Gustavsson, R. Leturcq, B. Simović, R. Schleser, T. Ihn, P. Studerus, K. Ensslin, D. C. Driscoll, and A. C. Gossard, *Phys. Rev. Lett.* **96** 076605 (2006)
  - [18] A. Jacobsen, P. Simonet, K. Ensslin, and T. Ihn, *N. J. Phys.* **14** 023052 (2012)
  - [19] C. W. J. Beenakker, *Phys. Rev. B* **44**, 1646 (1991)
  - [20] S. Machlup, *J. Appl. Phys.* **25**, 341 (1954)
  - [21] I. O. Kulik and R. I. Shekhter, *Sov. Phys. JETP* **41**, 308 (1975)
  - [22] Directly fitting the number of events yields a temperature of  $T = 2.61 \pm 0.03$  K for the single-level and  $T = 2.09 \pm 0.03$  K for the multi-level regime. The peak height thus extracted was used for the calculated curves.
  - [23] This method neglects the capacitive coupling between the source lead and the dot, which may alter the numerical value of the lever arm and thus the extracted temperature. This in turn may stretch or squeeze the graphs with respect to the energy axis but the shape and mutual position of both, experimental and calculated curves will remain unchanged.